IEEE Access
Multidisciplinary | Rapid Review | Open Access Journal

Received March 26, 2020, accepted April 13, 2020, date of publication May 6, 2020, date of current version May 19, 2020.

Digital Object Identifier 10.1109/ACCESS.2020.2992792

Bicycle Robot Balance Control Based on a Robust Intelligent Controller

CHIH-HUI CHIU AND CHI-YUAN WU

Department of Communications, Navigation and Control Engineering, National Taiwan Ocean University, Keelung 20224, Taiwan

Corresponding author: Chih-Hui Chiu (chchiu@ntou.edu.tw)

ABSTRACT In recent years, human assistant transportation systems have received much attention. Based on a microprocessor, a bicycle robot (BR) is designed and implemented in this work. In this study, a robust intelligent backstepping tracking control (RIBTC) system combined with an adaptive output recurrent Takagi-Sugeno-Kang type cerebellar model articulation controller (AORTSKCMAC) and a robust controller for BRs is implemented. The bicycle robot can maintain balance when subjected to a disturbance and still go forward. The proposed RIBTC is proposed to control the lean angle of the BR. The BRs can stably stand even with external disturbances. The development of the proposed controller is combined with a backstepping technique, the adaptive output recurrent TSKCMAC and a robust control method. The adaptive output recurrent TSKCMAC is used to mimic the ideal backstepping controller (IBC) because an accurate mathematical model of the system is hard to obtain. In general, the optimal values of system parameters can be calculated based on system dynamics when the system model is always known. However, the exact system dynamics are not always known. The parameters of the adaptive output recurrent TSKCMAC are tuned online in this study. The robust controller is designed to attenuate the effect of the residual approximation errors. Moreover, the Lyapunov function is used to verify the stability and convergence of the controller. The main contributions of this work include (1) the successful design and implementation of BR hardware and (2) the successful realization of the proposed RIBTC control scheme to control the BR. Finally, the experimental results demonstrate the effectiveness of the proposed control scheme for bicycle robot systems with unknown dynamic functions.

INDEX TERMS Bicycle robot, backstepping control, TSK CMAC, Lyapunov function, real-world control.

I. INTRODUCTION

Recently, many studies on the topic of the balance control of two-wheeled vehicles have been proposed. In particular, the balance control of an unmanned bicycle interests many researchers. There are many methods used for balance control of a riderless bicycle. In [1], the running motion of an electrical bicycle was stabilized using a bicycle's center of gravity and steering handle angle control. The authors in [2] used a gyroscopic balancer based on a fuzzy sliding mode controller to control a riderless bicycle. Yang and Murakami [3] proposed a method to control the steering of electric motorcycles. The motorcycle could self-balance by keeping its wheels at sway. A riderless bicycle was developed with a gyroscopic balancer controller by combining a fuzzy sliding mode controller with an adaptive fuzzy sliding mode controller [4]. In [5], the authors proposed a design method for steering control to maintain the balance of a bicycle.

High speed and accurate motion are necessary in modern control systems. Such performance can be realized using a mechanical transmission with rotary motors. These transmission parts obviously reduce the linear speed and system response but also generate chatter and friction. In some applications, simplification in actuation systems is a popular research topic. This can reduce the system cost, energy consumption, mechanical structure design and system uncertainty. A system with actuators that operate within their degrees of freedom is called an underactuated system. Underactuated systems can be found in many control applications such as biped robots, helicopters and inverted pendulums. For some applications, underactuated systems may be designed to sufficiently respond to actuator breakdowns.

Many studies have examined the system control of inverted pendulums. The inverted pendulum is an example of an

The associate editor coordinating the review of this manuscript and approving it for publication was Jun Shen.

underactuated and highly unstable system. Recently, many extensions of the one-dimensional inverted pendulum control system have been proposed. The most challenging task is to control such an inverted pendulum system when a cart is no longer on a guide rail. Obviously, the controller design becomes more difficult because of the physical structure.

In [6], a novel automatic motion control algorithm was investigated for wheeled inverted pendulum control. The developed scheme achieved dynamic balance and the desired motion tracking. In [7], the authors proposed an approach to compensate for external disturbances and model uncertainties to improve the system performance. The authors presented optimal motion planning for minimizing the energy consumption of a wheeled mobile robot in [8]. In [9], the authors proposed a novel smooth time-invariant controller to achieve desired position control and stabilization of an unstable pendulum-like central body.

On the control view, intelligent control theories (genetic algorithms, fuzzy controls, neural networks, or cerebellar model articulation controllers…etc) [10]–[20] provide a method for the design of online controllers of nonlinear systems with unknown or uncertain system dynamics. Many researchers have argued that neural networks (NNs) are powerful building blocks for a wide class of complex nonlinear system control strategies when model information is absent or when a controlled plant is considered a ''black box''. However, learning is slow because all system parameters are updated during each learning cycle. Therefore, the appropriateness of NNs is limited for problems requiring online learning. Recently, a cerebellar model articulation controller (CMAC) was proposed. In general, simple computation, fast learning, good generalization capability, and easier hardware implementation are the major advantages of a CMAC. However, the main drawback of CMACs is that they are static networks.

Recently, the backstepping controller has become a popular topic for nonlinear systems [21]–[22]. The main idea of backstepping controller design is to recursively choose some appropriate functions of state variables, which are used as fictitious control inputs for lower-dimension subsystems of the entire system. Each backstepping stage creates a new virtual control design, which is represented by the virtual control design of the previous design stages. The process terminates the feedback design of the real control input, which achieves the goal of original design by the final Lyapunov function, which is formed by summing the Lyapunov functions associated with each individual design stage. Therefore, the backstepping control method can maintain robustness with respect to uncertainty.

In this study, bicycle robot (BR) balance control based on robust intelligent backstepping tracking control (RIBTC) is proposed. A BR can be considered an inverted pendulum on the bicycle lean axis. This motion is achieved using a flywheel and a mechanical transmission with reduction gears and a lead screw. These transmission components markedly reduce the linear speed and dynamic response but also generate backlash and considerable friction. Clearly, this configuration has transmission loss. Conventional control technologies always require a good understanding of a plant. Undoubtedly, this system has many nonlinear components. Therefore, the dynamic model for such a system will be nonlinear, and the motor parameters are time-varying due to increased temperature and motor drive changes during operation. Obviously, BR control becomes arduous when using traditional control techniques because its exact system model is difficult to understand.

The RIBTC includes an adaptive output recurrent Takagi-Sugeno-Kang cerebellar model articulation controller (AORTCMAC) and a robust controller. The AORTCMAC is used to mimic an ideal backstepping control, and the robust H^{∞} controller is designed to attenuate the effect of the residual approximation errors and external desired attenuation level. The output recurrent Takagi-Sugeno-Kang cerebellar model articulation controller is a modified version of the traditional CMAC network such that a small number of receptive fields are used to capture the system dynamics, convert the static CMAC into a dynamic controller and add the Takagi-Sugeno-Kang fuzzy model, which has good capability for nonlinear systems. Combining the advantages of the above, AORTCMAC can aptly mimic an ideal backstepping controller.

In this study, RIBTC is used to control BRs. To obtain the optimal values of the system parameters, all parameter adaptation laws of the AORTCMAC are tuned online based on the Lyapunov stability theorem. The Taylor linearization technique and H^{∞} control technology are used; hence, the stability of the proposed controller can be guaranteed. In addition, the learning rate of the adaptation parameters is also determined by the Lyapunov function to ensure the convergence of tracking errors. The major contributions of this work include (1) the successful design and implementation of BR hardware and (2) the successful realization of the proposed RIBTC control scheme to control BRs. Finally, the effectiveness of the proposed control scheme for bicycle robot systems is demonstrated by several experimental results.

II. THE BICYCLE ROBOT PLATFORM HARDWARE STRUCTURE

This section introduces the hardware structure of a BR. Fig. 1 shows the degrees of freedom of the BR. The motions of the BR in this study maintain the balance at a fixed point. Therefore, the BR needs to maintain balance along the Z-axis. In this case, it has one degree of freedom. There are two state-space variables used to fully describe the dynamics of the BR. The dynamics of the BR are derived by assessing the BR as a reaction-wheel inverted pendulum. Obviously, the BR is a complex nonlinear system. For simplification, the flywheel and robot body are assumed to be a single body in this study.

A BR can be considered a reaction-wheel inverted pendulum, which is a nonlinear unstable system. The BR is divided into two subsystems: mechanism and hardware.

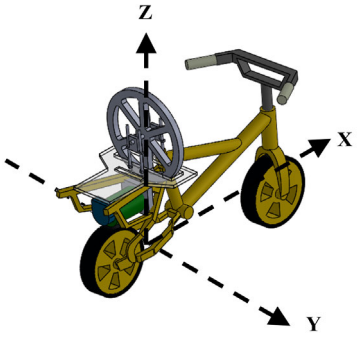

FIGURE 1. The degrees of freedom of BRs.

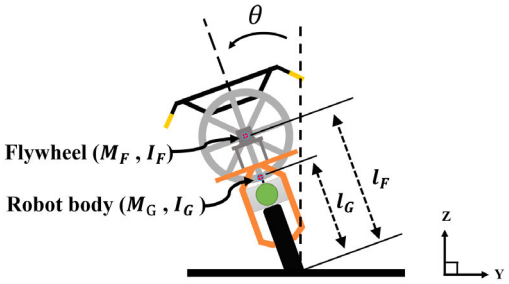

FIGURE 2. Definition variables of the dynamic model.

The mechanism of BR contains a frame, a motor and a flywheel. A child's bicycle is used as the skeleton for loading the whole system to conduct experiments. A 48 V planetary gear motor provides torque through the flywheel to maintain the balance of the BR. The hardware of the BR includes inertial measurement units (IMUs), a micro control unit and motor drive module. The main IMUs in this study are inclinometers and gyroscopes. The inclinometer measures the lean angle, and the gyroscope measures the change rate of the lean angle. A micro control unit (Arduino mega 2560) is used to acquire system states, realize the control algorithm and send out the control signals. To achieve the motor forward-reverse transfer, an H-bridge circuit is designed to drive the motor. To control the speed of the motor, pulse width modulation (PWM) techniques are used to control the motor. A 0–48 V PWM square wave signal at 490 Hz is sent to drive the motor. With these outlined features, the BR can maintain balance. Generally, the Arduino mega 2560 unit is suitable for control algorithm implementation and system control. The 48 V DC motor for the flywheel is placed on the BR system. This motor is sufficient for system control. However, it is uncontrollable if a large extra disturbance is exerted because the extra disturbance will exceed the ability to maintain system stability. In this case, the BR will be uncontrollable. In this study, the proposed BR can afford a maximum lean angle of under 5 degrees.

The Lagrange method is used to derive the dynamic model of the BR. Fig. 2 shows the variable definition of the dynamic model of the BR. Here, two variables require control to achieve a BR balance. One is the lean angle of the BR (θ), and the other is the change rate of the lean angle of the BR ($\dot{\theta}$).

The parameters used for BR are as follows.

M_F: Mass of the flywheel

M_G: Mass of the body

I_F: Moment of inertia of flywheel

I_G: Moment of inertia of the body about the center of the robot

l_F: Distance between the center of the flywheel and ground

l_G: Distance between the center of the robot body and ground

g: Acceleration of gravity

To obtain the dynamic equation from the Lagrange equation, the potential energy V and kinetic energy T are needed. V is the energy of that an object in a force field has due to its position. T is in the energy an object has due to its motion. It includes translational kinetic energy and rotational kinetic energy. The potential energy can be represented as equation (1). The total kinetic energy is obtained as the sum of translational kinetic energy and rotational kinetic energy as equation (2).

$$V = (m_G l_G + m_F l_F) g \cos\theta \tag{1}$$

$$T = (m_G l_G^2 + m_F l_F^2)\dot{\theta}^2. \tag{2}$$

Therefore, the Lagrange equation L can be represented as

$$\begin{aligned} L &= T - V \\ &= (m_G l_G^2 + m_F l_F^2) \times \dot{\theta}^2 - (m_G l_G + m_F l_F) g \cos\theta. \end{aligned} \tag{3}$$

Substituting L into the Lagrange dynamic equation, the dynamic equations of the system are obtained as equation (4).

$$\frac{d}{dt}\left(\frac{\partial L}{\partial \dot{\theta}}\right) - \frac{\partial L}{\partial \theta} = \tau_G. \tag{4}$$

where τ_G denotes the reaction torque caused by the flywheel. From equations (1), (2), (3) and (4), the dynamic equation is represented as equation (5).

$$\ddot{\theta} = \frac{(m_G l_G + m_F l_F) g \sin\theta}{2(m_G l_G^2 + m_F l_F^2)} + \frac{1}{2(m_G l_G^2 + 2m_F l_F^2)} \tau_G \tag{5}$$

After linearizing the system model of the BR in approximately $\theta \approx 0^\circ$ and $\dot{\theta} \approx 0^\circ$/ sec, the dynamic equation of the system body can be expressed as

$$\ddot{\theta} = \frac{(m_G l_G + m_F l_F) g}{2(m_G l_G^2 + m_F l_F^2)} \theta - \frac{k_{torque}}{2(m_G l_G^2 + 2m_F l_F^2)} \tau_F \tag{6}$$

where τ_F is the torque generated by the flywheel. The relationship between τ_G and τ_F can be expressed as $\tau_G = k_{(torque)}\tau_F$. It can be learned from the actual test that they move in opposite directions, and the value of τ_G is approximately 0.8 times that of τ_F.

III. CONTROLLER DESIGN

Let us consider BRs where the dynamic equation is described as follows:

$$\dot{x}_1(t) = x_2(t) \tag{7}$$
$$\dot{x}_2(t) = f(x,t) + g(x,t)u(t) + d(t) \tag{8}$$

where $X = [x_1(t), x_2(t)]^T = [x, \dot{x}]^T$ is the state vector of the system that is available through measurement. $f(x,t)$ and $g(x,t)$ represent the nonlinear uncertain functions that are assumed to be bounded, $u(t) \in R$ is the control input, and $d(t) \in R^n$ denotes an unknown but bounded external disturbance. (7) and (8) can be reformulated as follows:

$$\dot{x}_1(t) = x_2(t) \tag{9}$$
$$\begin{aligned}\dot{x}_2(t) &= f_0(x,t) + \Delta f(x,t) + [g_0 + \Delta g(x,t)]u(t) + d(x,t) \\ &= f_0(x,t) + g_0 u(t) + l(t)\end{aligned} \tag{10}$$

where $f_0(x,t)$ and g_0 denote the nominal parts, $\Delta f(x,t)$ and $\Delta g(x,t)$ are the unknown uncertainties of $f(x,t)$ and $g(x,t)$, respectively, and $l(t)$ represents lumped uncertainty, which is defined as $l(t) = \Delta f(x,t) + \Delta g(x,t)u(t) + d(x,t)$. It is essential that the constant $g_0 \neq 0$ for all x and t. It is supposed that $0 < g_0 < \infty$ for all x and t.

The control objective is to design a suitable control law for (8) so that X can track a reference trajectory vector $X_d = [x_{d1}(t), x_{d2}(t)]^T = [x_d, \dot{x}_d]^T$. If $f_0(x,t)$, g_0 and $l(x,t)$ are clearly known, an ideal backstepping controller (IBC) can be designed.

The system model of BRs cannot always be obtained precisely. To overcome this problem, a robust intelligent backstepping tracking control (RIBTC) system has been proposed for the systems.

A. ARTICULATION OF THE OUTPUT RECURRENT TAKAGI-SUGENO-KANG CEREBELLAR MODEL ARTICULATION CONTROLLER

A dynamic output recurrent Takagi-Sugeno-Kang cerebellar model articulation controller (ORTSKCMAC) neural network is proposed.

1) Input space X: X is a continuous n-dimensional input space. For a given $X = [x_1, x_2, \cdots, x_n]^T \in \Re^n$, the state variable of each input $x_i, i = 1, 2, \cdots, n$, must be divided into discrete regions, which are called elements. The number of elements is defined as n_E and is termed as a resolution.

2) Associative memory space A: Different elements can form a block. The number of blocks n_B is usually equal to or greater than two in a CMAC. A represents an associative memory space in which n_A ($n_A = n \times n_B$) constituents. In this space, the Gaussian function is accepted as the basis function here, which can be expressed as

$$\varphi_{ik} = \exp\left[\frac{-(x_{ri} - m_{ik})^2}{v_{ik}^2}\right], \quad for\ k = 1, 2, \cdots n_B \tag{11}$$

where φ_{ik} is the k-th block for the i-th input x_{ri} with mean m_{ik} and variance v_{ik}. In addition, the input of this block can be represented as

$$x_{ri}(N) = x_i(N) + r_i y(N-1) \tag{12}$$

where r_i is the recurrent weight of the recurrent unit. $y(N-1)$ denotes the past information of the network. It is clear that the input of this block contains the memory terms, which store the past information of the network. It captures system dynamics and converts the static CMAC into a dynamic controller. It will achieve good performance for nonlinear unknown systems.

3) Receptive-field space R: The areas formed by blocks are called receptive fields. The number of receptive fields is n_R. Its multidimensional basis function is as follows:

$$b_k(x, m_k, v_k) = \prod_{i=1}^{n} \varphi_{ik} = \exp\left[-\left(\sum_{i=1}^{n} \frac{(x_{ri} - m_{ik})^2}{v_{ik}^2}\right)\right] \quad for\ k = 1, 2, \cdots, n_B \tag{13}$$

where b_k is a receptive field formed by the k th basis function. The multidimensional receptive-field function can be expressed in vector type as follows:

$\psi(x, m, v, r) = [b_1, \cdots, b_k, \cdots, b_{n_R}]^T$ where $m = [m_1^T, \cdots, m_k^T, \cdots, m_{n_R}^T]^T \in \Re^{nn_R}$, $v = [v_1^T, \cdots, v_k^T, \cdots, v_{n_R}^T]^T \in \Re^{nn_R}$ and $r = [r_1^T, \cdots, r_k^T, \cdots, r_{n_R}^T]^T \in \Re^{nn_R}$.

4) TSK space T: This space is the linear combination function in the consequent part of the fuzzy system. Each location of the receptive field R can be converted to a linguistic variable with n_R components in the TSK space. The basic configuration of the TSK space includes a fuzzy rule base that is composed of a collection of fuzzy IF-THEN rules in the following.

$$\begin{aligned} Rule_\lambda &: \ If\ x_{r1}\ is\ F_1^\lambda, \cdots, x_{rn}\ is\ F_i^\lambda,\ then \\ \phi_\lambda &= q_{0\lambda} + q_{1\lambda}x_{r1} + \cdots + q_{n\lambda}x_{rn} \\ &= [1, X^T]q_\lambda \\ &= q_{0\lambda}z_0 + q_{1\lambda}z_1 + \cdots + q_{n\lambda}z_n \\ &= Z^T q_\lambda \end{aligned} \tag{14}$$

where $Rule_\lambda$ denotes the λth rule and λ is the number of rules. F_i^λ are the fuzzy sets, $i = 1, 2, \cdots, n$, and q_λ is a vector of the adjustable factors of the consequence part of the fuzzy rules. Furthermore, ϕ_λ is the linguistic variable. It can be expressed as $\phi = [\phi_1, \phi_2, \cdots, \phi_{n_R}]$, $Z = [1, X^T]^T$.

5) Output space Y: The output of ORTSKCMAC is the algebraic sum of the network linkage, parameter update, and active weighting in weight memory space in each layer, and it is expressed as

$$\phi^T \psi = q^T \Gamma = u_{ORTSKCMAC} = y \tag{15}$$

where $q = [q_1^T, q_2^T, \cdots, q_{nR}^T]^T$, $\Gamma = [b_1 Z^T, b_2 Z^T, \cdots, b_k Z^T]^T$, and $u_{ORTSKCMAC}$ is the output of ORTSKCMAC.

B. ROBUST INTELLIGENT BACKSTEPPING TRACKING CONTROL

The design of the RIBTC system for a BR uncertain nonlinear system is described as follows.

The system tracking error is defined as

$$e_1(t) = x_{d1}(t) - x_1(t). \tag{16}$$

Then the derivative of tracking error can be represented as

$$\dot{e}_1(t) = \dot{x}_{d1}(t) - \dot{x}_1(t) = x_{d2}(t) - x_2(t). \tag{17}$$

$x_2(t)$ can be viewed as a virtual control in the above equation. The following stabilizing function is defined:

$$\alpha(t) = k_1 e_1(t) + x_{d2}(t) \tag{18}$$

where $k_1$is a positive constant. The first Lyapunov function is chosen as

$$V_1(t) = \frac{1}{2} e_1^2(t) \tag{19}$$

Define

$$\begin{aligned} e_2(t) &= \alpha(t) - \dot{x}_1(t) \\ &= k_1 e_1(t) + x_{d2}(t) - \dot{x}_1(t) \\ &= k_1 e_1(t) + \dot{e}_1(t) \end{aligned} \tag{20}$$

The derivative of $V_1(t)$ is

$$\begin{aligned} \dot{V}_1(t) &= e_1(t)\dot{e}_1(t) = e_1(t)[e_2(t) - k_1 e_1(t)] \\ &= -k_1 e_1^2(t) + e_1(t)e_2(t) \end{aligned} \tag{21}$$

Therefore, if $e_2(t) = 0$, $\dot{V}_1(t) = -k_1 e_1^2(t) \leq 0$ will be achieved.

The derivative of $e_2(t)$ is expressed as

$$\begin{aligned} \dot{e}_2(t) &= \dot{\alpha}(t) - \ddot{x}_1(t) \\ &= \dot{\alpha}(t) - [f_0(x,t) + g_0 u + l(t)] \end{aligned} \tag{22}$$

Another Lyapunov function is chosen as

$$V_2(t) = V_1(t) + \frac{1}{2} e_2^2(t) \tag{23}$$

Then, the derivative of $V_2\,(t)$ is

$$\begin{aligned} \dot{V}_2(t) &= \dot{V}_1(t) + e_2(t)\dot{e}_2(t) \\ &= -k_1 e_1^2(t) + e_1(t)e_2(t) + e_2(t)\dot{e}_2(t) \\ &= -k_1 e_1^2(t) + e_2(t)\,[e_1(t) + \dot{e}_2(t)] \\ &= -k_1 e_1^2(t) + e_2(t) \\ &\quad \times [e_1(t) + \dot{\alpha}(t) - f_0(x,t) - g_0 u(t) - l(t)] \end{aligned} \tag{24}$$

If the dynamic system is well known, the ideal backstepping control law can be obtained as

$$u_{IBC}^* = \frac{1}{g_0}\left[\dot{\alpha}(t) - f_0(x,t) - l(t) + e_1(t) + k_2 e_2(t)\right] \tag{25}$$

where k_2 is a positive constant. Substituting (25) into (24), the following equation can be obtained:

$$\dot{V}_2(t) = -k_1 e_1^2(t) - k_2 e_2^2(t) \leq 0 \tag{26}$$

However, the dynamic model cannot be obtained in detail. Therefore, the AORTSKCMAC is utilized to estimate IBC in this study.

Theorem 1: The adaptive laws of AORTSKCMAC are chosen as

$$\dot{\hat{q}} = \eta_q e_2(t)\hat{\Gamma}^T \tag{27}$$

$$\dot{\hat{m}} = \eta_m e_2(t) C \hat{q}^T \tag{28}$$

$$\dot{\hat{v}} = \eta_v e_2(t) H \hat{q}^T \tag{29}$$

$$\dot{\hat{r}} = \eta_r e_2(t) R \hat{q}^T \tag{30}$$

where η_q, η_m, η_v and η_r are positive constants and

$$C = \left[\frac{\partial b_1}{\partial m} \cdots\cdots \frac{\partial b_{n_R}}{\partial m}\right]\Bigg|_{m=\hat{m}} \in R^{nn_R \times n_R},$$

$$H = \left[\frac{\partial b_1}{\partial v} \cdots\cdots \frac{\partial b_{n_R}}{\partial v}\right]\Bigg|_{v=\hat{v}} \in R^{nn_R \times n_R},$$

$$R = \left[\frac{\partial b_1}{\partial r} \cdots\cdots \frac{\partial b_{n_R}}{\partial r}\right]\Bigg|_{r=\hat{r}} \in R^{nn_R \times n_R}.$$

The robust H^∞ controller is given as

$$u_R = \frac{(\delta^2 + 1)}{2\delta^2} e_2(t) \tag{31}$$

where δ is a positive constant. Then, the desired robust tracking performance can be achieved for a prescribed attenuation level δ.

Proof: Since the AORTSKCMAC is utilized to estimate IBC, $u_{AORTSKCMAC}$ can be written as

$$u_{AORTSKCMAC}\,(x, q, m, v, r) = y = q^T \Gamma(x, m, v, r) \tag{32}$$

Assume there is an optimal $u_{AORTSKCMAC}^*$ to approach the IBC such that

$$u_{IBC}^* = u_{AORTSKCMAC}(x,\ q^*,\ m^*, v^*, r^*) + \varepsilon = q^{*T}\Gamma^* + \varepsilon \tag{33}$$

where ε is a minimum estimation error and q^*, m^*, v^*, Γ^* and r^* are the optimal values of q, m, v, Γ, and r. Nevertheless, the optimal $u_{AORTSKCMAC}^*$ cannot be obtained, and the online estimation of $\hat{u}_{AORTSKCMAC}$ is used to estimate. u_{IBC}^*. The control law (28) can be rewritten as follows:

$$u = u_{AORTSKCMAC}(x,\ \hat{q},\ \hat{m},\ \hat{v},\ \hat{r}) + u_R = \hat{q}^T\hat{\Gamma} + u_R \tag{34}$$

where $\hat{q}$, $\hat{m}$, $\hat{v}$, $\hat{\Gamma}$ and $\hat{r}$ are the estimates of the optimal parameters q^{*T}, m^*, v^*, Γ^* and r^*. Subtracting (34) from (33), an approximation error $\tilde{u}$ is defined as

$$\begin{aligned} \tilde{u} &= u_{IBC}^* - u \\ &= q^{*T}\Gamma^* + \varepsilon - \hat{q}^T\hat{\Gamma} - u_R \\ &= \tilde{q}^T\Gamma^* + \hat{q}^T\tilde{\Gamma} + \varepsilon - u_R \end{aligned} \tag{35}$$

where $\tilde{q} = q^* - \hat{q}$ and $\tilde{\Gamma} = \Gamma^* - \hat{\Gamma}$. Furthermore, employing the linearization technique transforms the multidimensional receptive-field basis function into the partially linear form. The expansion of $\tilde{\Gamma}$ in the Taylor series can be obtained as

$$\tilde{\Gamma} = \begin{bmatrix} \tilde{b}_1 \\ \vdots \\ \tilde{b}_k \\ \vdots \\ \tilde{b}_{nR} \end{bmatrix} = \begin{bmatrix} (\frac{\partial b_1}{\partial m})^T \\ \vdots \\ (\frac{\partial b_k}{\partial m})^T \\ \vdots \\ (\frac{\partial b_{nR}}{\partial m})^T \end{bmatrix}\Bigg|_{m=\hat{m}}$$

$$\cdot (m^* - \hat{m}) + \left[\begin{array}{c} (\frac{\partial b_1}{\partial v})^T \\ \vdots \\ (\frac{\partial b_k}{\partial v})^T \\ \vdots \\ (\frac{\partial b_{nR}}{\partial v})^T \end{array}\right]\Bigg|_{v=\hat{v}} \cdot (v^* - \hat{v})$$

$$+ \left[\begin{array}{c} (\frac{\partial b_1}{\partial r})^T \\ \vdots \\ (\frac{\partial b_k}{\partial r})^T \\ \vdots \\ (\frac{\partial b_{nR}}{\partial r})^T \end{array}\right]\Bigg|_{r=\hat{r}} \cdot (r^* - \hat{r}) + O_t$$

$$= C^T\tilde{m} + H^T\tilde{v} + R^T\tilde{r} + O_t \tag{36}$$

where $\tilde{b}_k = b_k^* - \hat{b}_k$; b_k^* and $\hat{b}_k$ are the optimal and estimated parameters of b_k. $\tilde{m} = m^* - \hat{m}$; $\tilde{v} = v^* - \tilde{v}$; $O_t \in R^{n_R}$ is a vector of higher-order terms. Rewriting (36), it can be obtained that

$$\Gamma^* = \hat{\Gamma} + C^T\tilde{m} + H^T\tilde{v} + P^T\tilde{r} + O_t \tag{37}$$

Substituting (36) and (37) into (35) yields

$$\begin{aligned} \tilde{u} &= \tilde{q}^T(\hat{\Gamma} + C^T\tilde{m} + H^T\tilde{v} + R^T\tilde{r} + O_t) \\ &\quad + \hat{q}^T(C^T\tilde{m} + H^T\tilde{v} + R^T\tilde{r} + O_t) + \varepsilon - u_R \\ &= \tilde{q}^T\hat{\Gamma} + \hat{q}^T(C^T\tilde{m} + H^T\tilde{v} + R^T\tilde{r}) + \xi - u_R \end{aligned} \tag{38}$$

where $\xi = \tilde{q}^T\left[C^T\tilde{m} + H^T\tilde{v} + R^T\tilde{r}\right] + q^{*T}O_t + \varepsilon$.

To develop the robust H^∞ controller, the derivative of $e_2(t)$ can be expressed as

$$\begin{aligned} \dot{e}_2(t) &= g_0(u_{IBC}^* - u) - e_1(t) - k_2e_2(t) \\ &= g_0\tilde{u} - e_1(t) - k_2e_2(t) \\ &= g_0\left[\tilde{q}^T\hat{\Gamma} + \hat{q}^T(C^T\tilde{m} + H^T\tilde{v} + R^T\tilde{r})\right] \\ &\quad + \xi - u_R - e_1(t) - k_2e_2(t) \end{aligned} \tag{39}$$

The Lyapunov function is defined as

$$V_3(t) = V_2(t) + \frac{g_0}{2\eta_q}\tilde{q}\tilde{q}^T + \frac{g_0}{2\eta_m}\tilde{m}^T\tilde{m} + \frac{g_0}{2\eta_v}\tilde{v}^T\tilde{v} + \frac{g_0}{2\eta_r}\tilde{r}^T\tilde{r} \tag{40}$$

where η_1, η_2, η_3, and η_4 are positive constants. Taking the derivative of the Lyapunov function (40) and using (39) it is concluded that

$$\begin{aligned} \dot{V}_3(t) &= \dot{V}_2(t) + \frac{g_0}{\eta_q}\tilde{q}\dot{\tilde{q}}^T + \frac{g_0}{\eta_m}\dot{\tilde{m}}^T\tilde{m} + \frac{g_0}{\eta_v}\dot{\tilde{v}}^T\tilde{v} + \frac{g_0}{\eta_r}\dot{\tilde{r}}^T\tilde{r} \\ &= -k_1e_1^2(t) + e_2(t)\left[e_1(t) + \dot{e}_2(t)\right] - \frac{g_0}{\eta_q}\tilde{q}\dot{\hat{q}}^T \\ &\quad - \frac{g_0}{\eta_m}\dot{\hat{m}}^T\tilde{m} - \frac{g_0}{\eta_v}\dot{\hat{v}}^T\tilde{v} - \frac{g_0}{\eta_r}\dot{\hat{r}}^T\tilde{r} \\ &= -k_1e_1^2(t) - k_2e_2^2(t) + e_2(t)g_0 \\ &\quad \times \left\{\tilde{q}^T\hat{\Gamma} + \left[\hat{q}^T(C^T\tilde{m} + H^T\tilde{v} + R^T\tilde{r}\right] + \xi(t) - u_R\right\} \\ &\quad - \frac{g_0}{\eta_q}\tilde{q}\dot{\hat{q}}^T - \frac{g_0}{\eta_m}\dot{\hat{m}}\tilde{m} - \frac{1}{\eta_v}\dot{\hat{v}}\tilde{v} - \frac{1}{\eta_r}\dot{\hat{r}}\tilde{r} \\ &= -k_1e_1^2(t) - k_2e_2^2(t) + \left[\tilde{q}^T(e_2(t)\hat{\Gamma} - \frac{1}{\eta_q}\dot{\hat{q}}^T)g_0\right] \\ &\quad + \left[(e_2(t)\hat{q}^TC^T - \frac{1}{\eta_m}\dot{\hat{m}}^T)\tilde{m}g_0\right] \\ &\quad + \left[(e_2(t)\hat{q}^TH^T - \frac{1}{\eta_v}\dot{\hat{v}}^T)\tilde{v}g_0\right] \\ &\quad + \left[(e_2(t)\hat{q}^TR^T - \frac{1}{\eta_r}\dot{\hat{r}}^T)\tilde{r}g_0\right] + e_2(t)g_0(\xi(t) - u_R) \end{aligned} \tag{41}$$

If the adaptive laws of the AORTSKCMAC are chosen as (27)-(30) and (31), (41) can be rewritten as

$$\begin{aligned} \dot{V}_3 &= -k_1e_1^2 - k_2e_2^2(t) + g_0e_2(t)(\xi - \frac{\delta^2+1}{\delta^2}e_2(t)) \\ &= -k_1e_1^2(t) - k_2e_2^2(t) - \frac{1}{2\delta^2}g_0e_2^2(t) \\ &\quad - \frac{1}{2}g_0\left[e_2(t) - \xi(t)\right]^2 + \frac{1}{2}g_0\xi(t)^2 \\ &\le -\frac{1}{2\delta^2}g_0e_2^2(t) + \frac{1}{2}g_0\xi(t)^2 \end{aligned} \tag{42}$$

Assume $\xi \in L_2[0,T]$, $\forall T \in [0,\infty)$, Integrating the above equation from $t = 0$ to $t = T$, yields

$$V_3(T) - V_3(0) \le -\frac{1}{2\delta^2}g_0\int_0^T e_2^2(t)dt + \frac{1}{2}g_0\int_0^T \xi^2(t)dt \tag{43}$$

Since $V_3(T) \ge 0$, the above inequality implies the following inequality

$$\frac{1}{2\delta^2}g_0\int_0^T e_2^2(t)dt \le V_3(0) + \frac{1}{2}g_0\int_0^T \xi^2(t)dt \tag{44}$$

Using (40), the above inequality is equivalent to the following

$$\begin{aligned} \frac{1}{\delta^2}\int_0^T e_2^2(t)dt \le{}& \frac{e_1^2(0)}{g_0} + \frac{e_2^2(0)}{g_0} + \frac{1}{\eta_1}\tilde{q}(0)\tilde{q}^T(0) \\ &+ \frac{1}{\eta_2}\tilde{m}^T(0)\tilde{m}(0) + \frac{1}{\eta_3}\tilde{v}^T(0)\tilde{v}(0) \\ &+ \frac{1}{\eta_4}\tilde{r}^T(0)\tilde{r}(0) + \int_0^T \xi^2(t)dt \end{aligned} \tag{45}$$

If the system starts with initial condition $e_1(0) = 0$, $e_2(0) = 0$, $\tilde{w}(0) = 0$, $\tilde{m}(0) = 0$, $\tilde{v}(0) = 0$, $\tilde{r}(0) = 0$ the H^∞ tracking performance in (41) can be rewritten as

$$\sup_{\xi \in L_2[0,T]} \frac{||e_2||}{||\xi||} \le \delta \tag{46}$$

where $||e_2||^2 = \int_0^T e_2^2(t)dt$ and $||\xi||^2 = \int_0^T \xi^2(t)dt$. The attenuation constant δ can be specified by the designer to achieve the desired attenuation ratio between $||e_2||$ and $||\xi||$. If $\delta = \infty$, this is the case of minimum error tracking control without disturbance attenuation [20]. Then, the desired robust tracking performance in (46) can be achieved for a prescribed attenuation level δ.

Q.E.D.

Figure 3 shows the structure of the proposed control system.

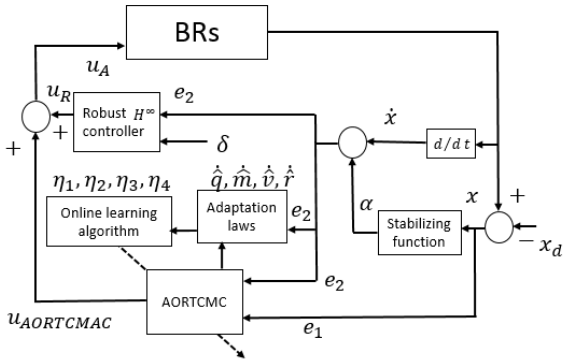

FIGURE 3. Bloch diagram of RIBTC.

C. CONVERGENCE ANALYSIS

The learning laws of equations (27) to (30) are arbitrary positive constants. Obviously, the learning laws of (27) to (30) need to call for a proper choice of the constants η_q, η_m, η_v and η_r. For a small value, the adaptive speed is slow. On the other hand, the performances of the intelligent backstepping system may not be good if the constants are too large. Definitely, it is difficult to choose suitable learning rates for the four adaptive laws in real-time control by the user. To choose those constants effectively, the variable learning constants, which guarantee the convergence of the output error, are given in the following.

Theorem 2: Let $\partial y/\partial s = Q_s(N)$ for $s = q, m, v$ *and* r, the convergence is guaranteed when η_s is chosen as

$$0 < \eta_s < \frac{2}{||Q_s(N)||^2[\delta_p/e_1(N)]^2} \tag{47}$$

where $\|\cdot\|$ is Euclidean norm. $\frac{\partial y}{\partial q} = Q_q(N)$, $\frac{\partial y}{\partial m} = Q_m(N)$, $\frac{\partial y}{\partial v} = Q_v(N)$, $\frac{\partial y}{\partial r} = Q_r(N)$. In this study, the learning rates can be obtained as

$$\eta_s = \frac{1}{||Q_s(N)||^2[\delta_p/e_1(N)]^2}. \tag{48}$$

Proof:

As $Q_s(N) = \frac{\partial y}{\partial s}$ for $s = q, m, v$ *and* r, this reveals that

$$Q_q(N) = \frac{\partial y}{\partial q} = \left[\frac{\partial y}{\partial q_{j1}}, \cdots, \frac{\partial y}{\partial q_{jk}}, \cdots, \frac{\partial y}{\partial q_{jn_R}}\right]^T \tag{49}$$

$$Q_m(N) = \frac{\partial y}{\partial m} = \left[\frac{\partial y}{\partial m_{11}}, \cdots, \frac{\partial y}{\partial m_{ik}}, \cdots, \frac{\partial y}{\partial m_{nn_R}}\right]^T \tag{50}$$

$$Q_v(N) = \frac{\partial y}{\partial v} = \left[\frac{\partial y}{\partial v_{11}}, \cdots, \frac{\partial y}{\partial v_{ik}}, \cdots, \frac{\partial y}{\partial v_{nn_R}}\right]^T \tag{51}$$

$$Q_r(N) = \frac{\partial y}{\partial r} = \left[\frac{\partial y}{\partial r_1}, \cdots, \frac{\partial y}{\partial r_i}, \cdots, \frac{\partial y}{\partial r_n}\right]^T. \tag{52}$$

Here, the Lyapunov function is chosen as

$$V(N) = \frac{1}{2}e_1^2(N) \tag{53}$$

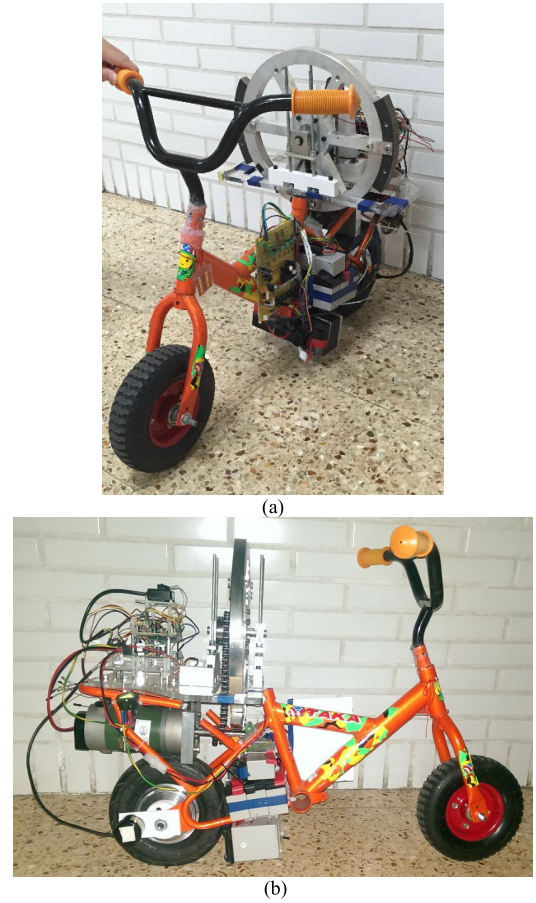

(a)

(b)

FIGURE 4. The BR experiment system. (a) Front view. (b) Side view.

The change of the Lyapunov function is obtained as

$$\Delta V(N) = V(N+1) - V(N) = \frac{1}{2}\left[e_1^2(N+1) - e_1^2(N)\right] \tag{54}$$

The error difference $e_1(N+1)$ can be expressed as follows

$$e_1(N+1) = e_1(N) + \Delta e_1(N) = e_1(N) + \left[\frac{\partial e_1(N)}{\partial s}\right]\Delta s \tag{55}$$

where it is obtained that

$$\frac{\partial e_1}{\partial s} = \frac{\partial e_1}{\partial x}\frac{\partial x}{\partial y}\frac{\partial y}{\partial s} = -\frac{\partial x}{\partial y}Q_s(N) \tag{56}$$

The error term to be propagated is given by [23]

$$\sigma_p = -\frac{\partial V}{\partial y} = -\frac{\partial V}{\partial e_1}\frac{\partial e_1}{\partial x}\frac{\partial x}{\partial y} = e_1\frac{\partial x}{\partial y} \tag{57}$$

Thus,

$$\begin{aligned} e_1(N+1) &= e_1(N) - \left[\frac{\sigma_p}{e_1(N)}Q_s(N)\right]^T \eta_s\sigma_p Q_s(N) \\ &= e_1(N)\left[1 - \eta_s(\frac{\sigma_p}{e_1(N)})^2||Q_s(N)||^2\right] \end{aligned} \tag{58}$$

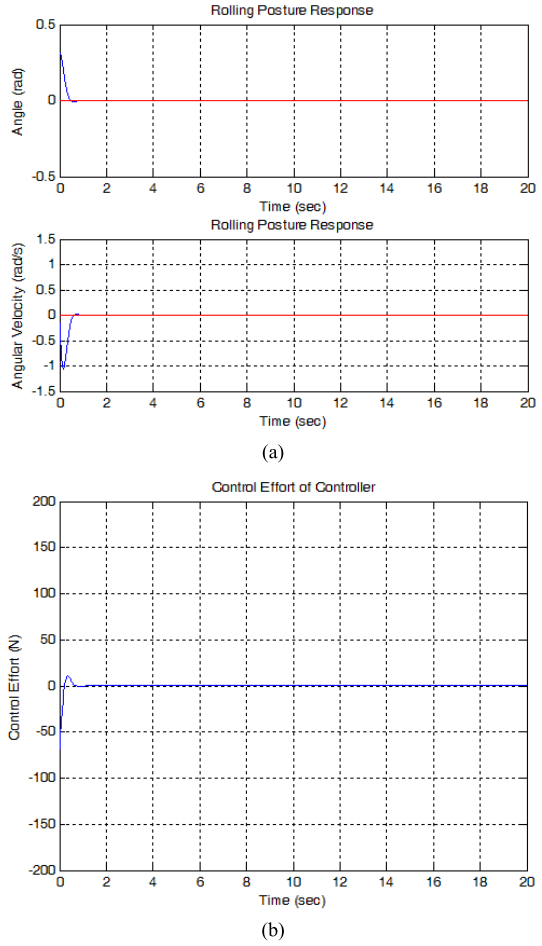

FIGURE 5. The system simulation response of the BR standing upright control with nonzero initial conditions: (a) The lean angle and the angular velocity of the BR. (b) The control effort of the BR.

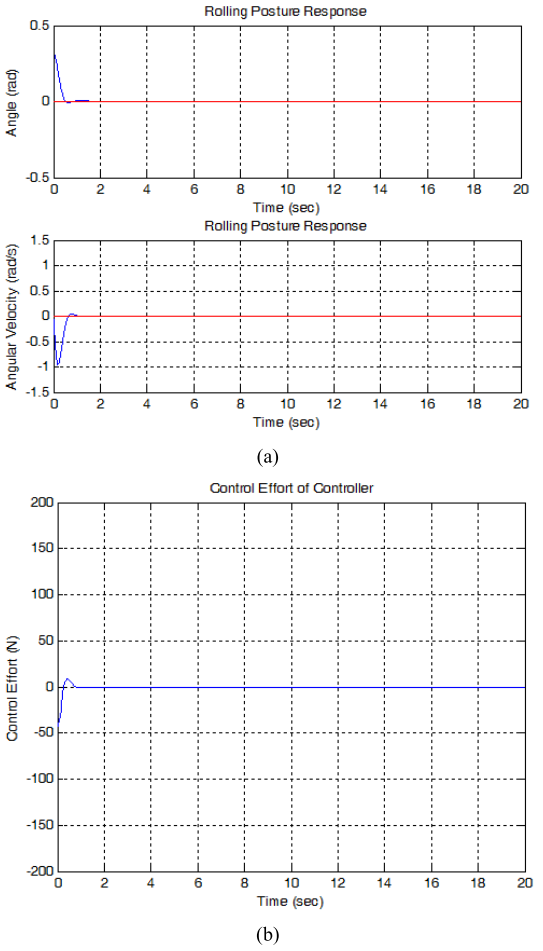

FIGURE 6. The system simulation response of the BR under the Case 2 situation: (a) The lean angle and the angular velocity of the BR. (b) The control effort of the BR.

From (54) and (58), $\Delta V(N)$ can be represented as

$$\Delta V(N) = \frac{1}{2}\eta_s \sigma_p^2 \parallel Q_s(N) \parallel^2 \left[\eta_s \left(\frac{\sigma_p}{e_1(N)}\right)^2 \parallel Q_s(N) \parallel^2 - 2\right] \tag{59}$$

If η_s is chosen as $0 < \eta_s < \frac{2}{||Q_s(N)||^2[\sigma_p/e_1(N)]^2}$, $\Delta V(N)$ in (59) is less than 0. Therefore, the Lyapunov stability of $V > 0$ and $\Delta V < 0$ is guaranteed. Thus, the tracking error $e_1(N)$ will converge to zero as $t \to \infty$. From the above derivation, $V > 0$ and $\Delta V < 0$, when $t \to \infty$, the stability of the Lyapunov function can be guaranteed.

Q.E.D.

IV. SEVERAL SYSTEM RESPONSES

The BR is controlled by using the RIBTC in this section. Photographs of the BR experimental system are shown in Fig. 4. Here, the reference signals x_d and $\dot{x}_d$ are all zero.

The parameters of the BR are given as follows: the total weight of the BR is approximately 19.7 kg (M_G is approximately 17.5 kg and M_F is approximately 2.2 kg), $l_{FO} = 0.42$m, and $l_{GO} = 0.2$m.

A. SIMULATION RESULTS

Here, the proposed AORTCMAC is characterized by $\rho = 4$, $n_E = 5$, and $n_B = n_R = 2 \times 4$. The initial conditions of the AORCMAC control system parameters are chosen as $k_1 = 5$, $m_{i1} = -0.21$, $m_{i2} = -0.15$, $m_{i3} = -0.09$, $m_{i4} = -0.03$, $m_{i5} = 0.03$, $m_{i6} = 0.09$, $m_{i7} = 0.15$, $m_{i8} = 0.21$ and $v_{ik} = 0.5$, with $r_{ik} = 0.005$ for all i and k. Moreover, $q_{11} = -10$, $q_{21} = -7.5$, $q_{31} = -5$, $q_{41} = -2.5$, $q_{51} = 2.5$, $q_{61} = 5$, $q_{71} = 7.5$, $q_{71} = 10$ and $q_{h2} = 5$, with $q_{h2} = 5$ for $h = 1, \cdots, 8$. The adaptive laws of RIBTC are chosen as Eqs. (27)-(30). The attenuation level $\delta = 0.5$. Moreover, according to Theorem 2, the proposed variable learning-rates are selected.

1) CASE 1: BALANCE CONTROL WITH NONZERO INITIAL CONDITIONS

In this case, a standing upright balance control is tested, and its target lean angle of the BR is 0 degrees. The control system initial parameters shown above are considered. The system performance is shown in Fig. 5. The initial value of the system lean angle is given as $\pi/10$. In Fig. 5(a), the lean

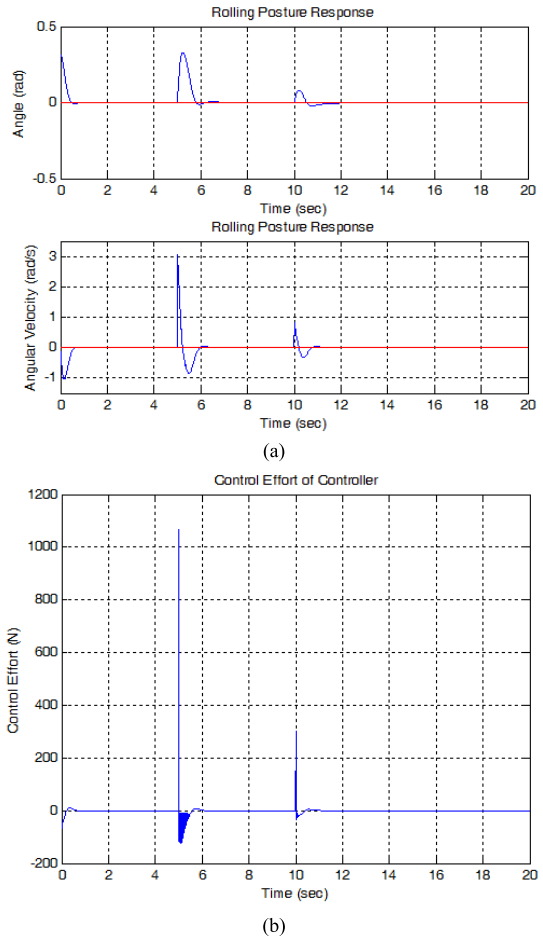

FIGURE 7. The system simulation response of the BR under the Case 3 situation: (a) The lean angle and the angular velocity of the BR. (b) The control effort of the BR.

angle of the BR converges to 0 degrees at approximately 1 second. Moreover, the angular velocity of the BR also converges at approximately 1 second. The control effort of the BR is shown in Fig. 5(b). Clearly, the vehicle can stand upright stably.

2) CASE 2: BALANCE CONTROL WITH DIFFERENT INITIAL PARAMETERS

In this case, balance control with nonzero initial conditions is performed again. However, the means of the antecedent part of the Gaussian membership functions are set to other values. For different parameter initial conditions testing, the initial conditions of the AORCMAC control system parameters are given as $m_{i1} = -0.63$, $m_{i2} = -0.45$, $m_{i3} = -0.27$, $m_{i4} = -0.09$, $m_{i5} = 0.09$, $m_{i6} = 0.27$, $m_{i7} = 0.45$ and $m_{i8} = 0.63$. The system performance is shown in Fig. 6.

Comparing Fig. 5(a) with Fig. 6(a), the difference is small. In this case, the proposed controller can deal successfully with the effect of the initial parameter setting. Fig. 6(b) shows the control effort of the BR.

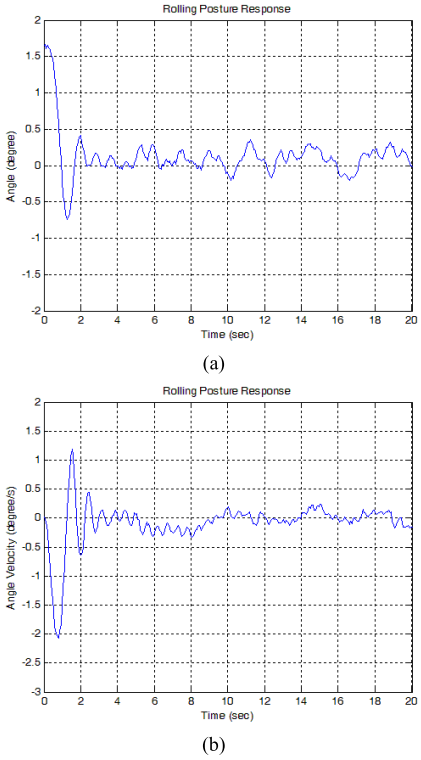

FIGURE 8. The system performance of the BR balance control at a fixed point. (a) The lean angle of the BR. (b) The angular velocity of the BR.

3) CASE 3: THE EFFECT OF BALANCE CONTROL WITH PARAMETER UNCERTAINTIES ON THE DYNAMIC RESPONSE

In this case, balance control is performed again. However, at 5 seconds, the angle error of the BR is given as 0.1. Moreover, at 10 seconds, the BR system input is suddenly 300. The system response is shown in Fig. 7. The largest differences are shown at 5 seconds and 10 seconds in Fig. 7(a). However, the angle trajectory finally converges to the intended target position. Obviously, in this case, the proposed controller can deal successfully with the effect of parameter uncertainties. Fig. 7(b) shows the control effort of the BR.

B. EXPERIMENTAL RESULTS

The proposed AORTCMAC in experimental testing is also characterized by $\rho = 4$, $n_E = 5$, and $n_B = n_R = 2 \times 4$. The initial conditions of the AORCMAC control system parameters are chosen as $k_1 = 0.8$, $r_1 = 0.1$, $r_2 = 0.1$, $m_{i1} = -3$, $m_{i2} = -2$, $m_{i3} = -1$, $m_{i4} = -0.5$, $m_{i5} = 0.5$, $m_{i6} = 1$, $m_{i7} = 2$, $m_{i8} = 3$ and $v_{ik} = 1.9$ for all i and k. Moreover, $q_{11} = -1.5$, $q_{21} = -1.125$, $q_{31} = -0.75$, $q_{41} = -0.375$, $q_{51} = 0.375$, $q_{61} = 0.75$, $q_{71} = 1.125$, $q_{71} = 1.5$ and $q_{h2} = 0.15$, with $q_{h2} = 0.15$ for $h = 1, \cdots, 8$. The adaptive laws of RIBTC are chosen as Eqs. (27)-(30). The attenuation level $\delta = 1$. The control interval is set to 1.5 ms. Moreover, according to Theorem 2, the proposed variable learning rates are selected.

Generally, the Arduino mega 2560 unit is suitable for control algorithm implementation and system control. A 48 V DC

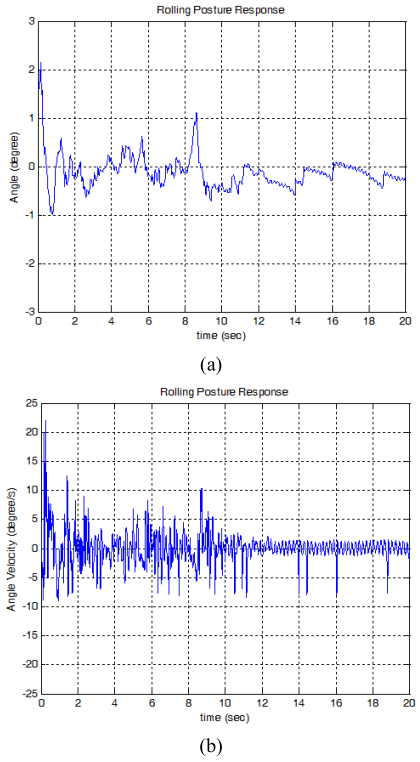

FIGURE 9. The system performance of the BR balance control for FLC. (a) The lean angle of the BR. (b) The angular velocity of the BR.

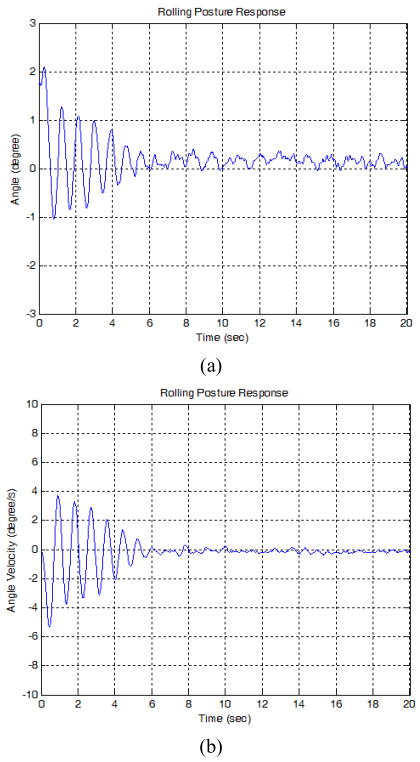

FIGURE 10. The system performance of the BR balance control for PID. (a) The lean angle of the BR. (b) The angular velocity of the BR.

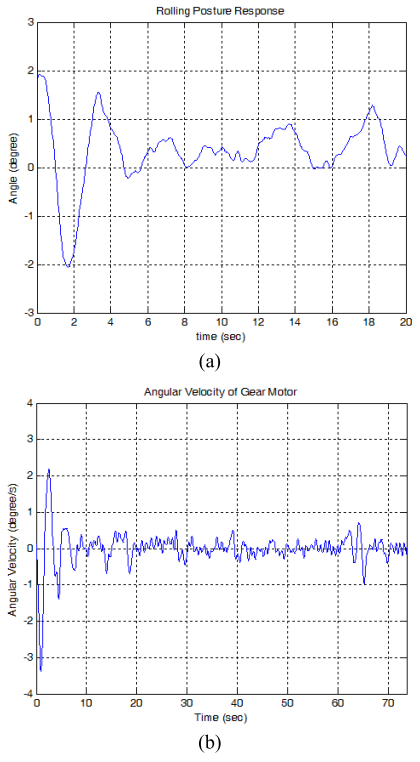

FIGURE 11. The system performance of the BR balance control for ENN. (a) The lean angle of the BR. (b) The angular velocity of the BR.

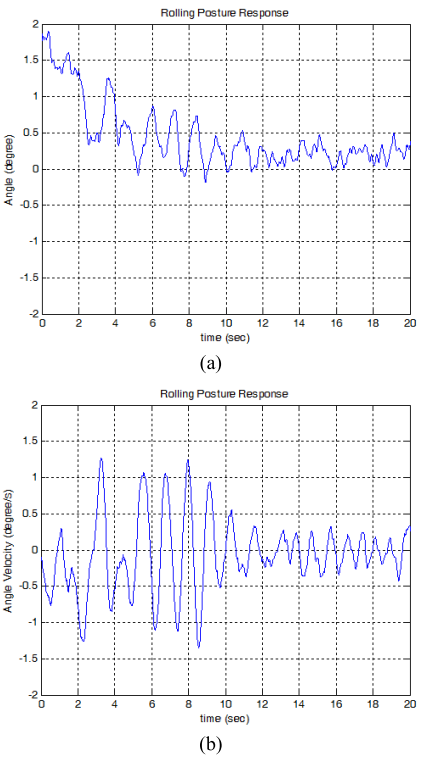

FIGURE 12. The system performance of the BR balance control for TS fuzzy control. (a) The lean angle of the BR. (b) The angular velocity of the BR.

motor for the flywheel is also sufficient for system control. However, it is uncontrollable if a large extra disturbance is exerted. In this subsection, the maximum lean angle of the BR is limited to less than 5 degrees.

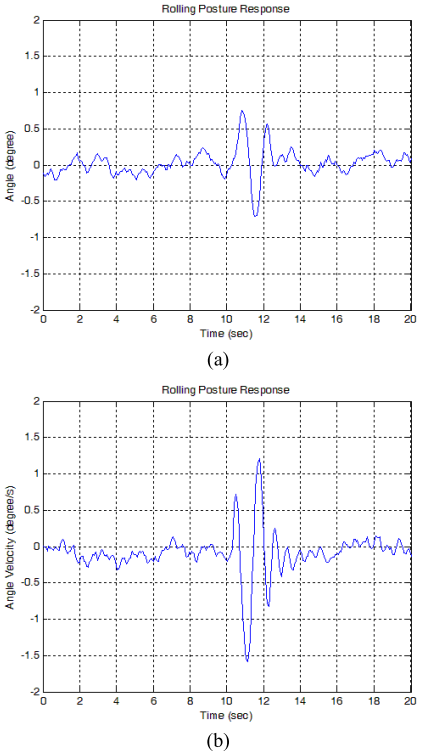

FIGURE 13. The system performance of the BR balance control with lateral external disturbance. (a) The lean angle of the BR. (b) The angular velocity of the BR.

1) BALANCE CONTROL EXPERIMENT

In this case, the BR starts at approximately 1.5 degrees on indoor flat ground. After 20 seconds, the experimental test stopped. The BR is required to stay at the origin point. Figure 8 shows the experimental results. The lean angle is shown in Fig. 8(a). Figure 8(b) shows the angular velocity of the BR. Obviously, the lean angle approaches zero degrees at approximately 2 seconds. Then, the BR stands stably.

For comparison, the classic PID, the fuzzy logic control (FLC), the Elman neural network (ENN) [23], and the Takagi–Sugeno (TS) fuzzy control schemes [24] are used to control the BR. In the Mamdani-like fuzzy controller, the Gaussian function is used as the membership function of the antecedent part. The consequent part is a singleton. The chosen parameters of the classic PID controller are: $k_p = 0.2$, $k_i = 0.1$ and $k_d = 0.2$. The parameters of the AFSMC method are: $\gamma_f = 0.3$, $\gamma_g = 0.2$, $\gamma_k = 0.001$ $c_1 = 10$, $g_{\max} = 1.46$, $g_{\min} = 0.74$, and $F = 16$. Moreover, the normalization factor of the fuzzy control term is $K_{afs} = 5$.

In this case, the BR starts at approximately 1.5 degrees on indoor flat ground. After 20 seconds, the experimental test stopped. The BR is required to stay at the origin point. Figure 8 shows the experimental results. The lean angle is shown in Fig. 8(a). Figure 8(b) shows the angular velocity of the BR. Obviously, the lean angle approaches zero degrees at approximately 2 seconds. Then, the BR stands stably.

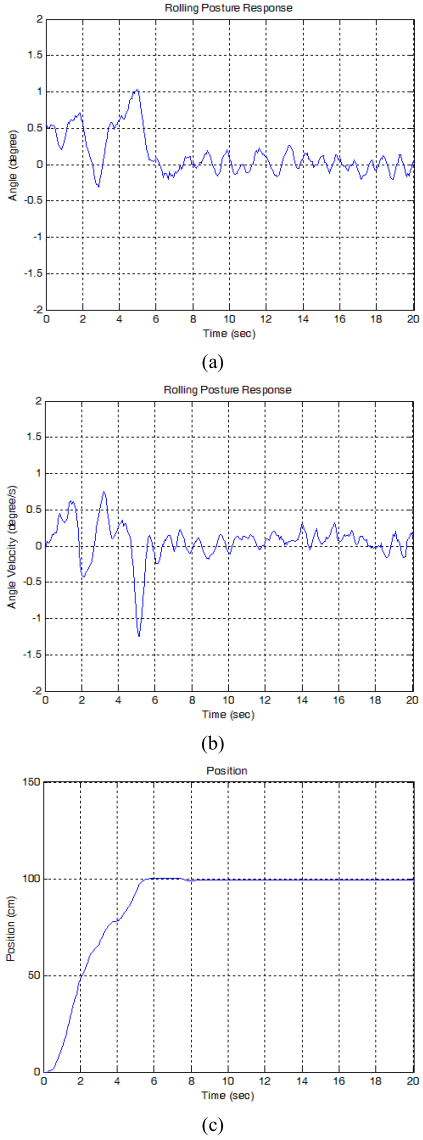

FIGURE 14. The system performance of the BR moving balance control. (a) The lean angle of the BR. (b) The angular velocity of the BR. (c) BR position.

For recording the respective control performances, the root-mean-square-error (RMSE) [21] for the angle tracking errors is defined as:

$$RMSE = \sqrt{\frac{1}{N}\sum_{i=1}^{N} e_1(i)^2} \tag{60}$$

where $N = 4000$ is sampling times for the angle tracking errors. The unit of RMSE is degrees. The experimental performance comparisons of the classic PID, the fuzzy control method, the ENN, and the TS fuzzy control scheme are summarized in Table 1.

According to the RMSE measures in Table 1, the proposed control scheme has the minimum RMSE.

Based on the above experimental results and Table 1, the RIBTC control system can achieve good control

TABLE 1. Performance comparisons.

Performance / Control condition	RIBTC	TS fuzzy control	Fuzzy control	PID	ENN
Balance control	0.3438	0.3893	0.3647	0.4391	0.5533

performance for the BR compared with the other methods. The proposed controller is suitable for BR real-time control.

2) LATERAL EXTERNAL DISTURBANCE EXPERIMENT

In this test, the BR starts at approximately 0 degrees on indoor flat ground. When the BR tends to stabilize, the external disturbance is given at approximately 11 seconds. The control process lasts for 20 seconds. Figure 13 shows the experimental performance. The lean angle of the BR is shown in Fig. 13(a). Figure 13(b) shows the angular velocity of the BR. It is obvious that the BR leans to 0.5 degrees when an external disturbance is exerted. Then, the BR tends to -0.5 degrees immediately. At approximately 13 seconds, the BR returns to stable status. Obviously, the BR stabilizes quickly.

3) MOVING BALANCE EXPERIMENT

The BR starts at approximately 0.5 degrees and goes to 100 cm before the start point on indoor flat ground. The BR reaches the target position at approximately 6 seconds, and then the BR stays in the target position stably until 20 seconds. Figure 14 shows the system performance of the BR moving forward control experiment. In Fig. 14(a), the lean angle of the BR has a large variation when the BR moves forward. After 6 seconds, the lean angle of the BR is maintained at approximately 0 degrees.

Obviously, good control performance is achieved by the proposed controller shown in the above experimental results. This means that the RIBTC is suitable for real-time BR control. Figure 15 shows a sequence of experimental photographs for the external disturbance test.

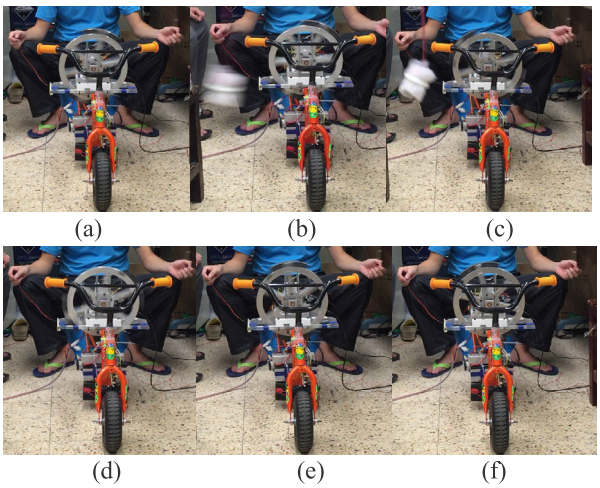

FIGURE 15. The sequence of experiments.

V. CONCLUSION

In this study, a BR real-world control system has been successfully implemented. The proposed intelligent controller is designed to maintain the bicycle balance. When the BR is hit by an external disturbance, the controller can still prevent the system from falling down. The main contributions of this work include (1) the successful design and implementation of a BR hardware, and (2) the successful realization of the proposed RIBTC control scheme to control the BR. The experimental results verify that the proposed control schemes are effective for BR real-world control.

REFERENCES

[1] C.-L. Hwang, H.-M. Wu, and C.-L. Shih, "Fuzzy sliding-mode underactuated control for autonomous dynamic balance of an electrical bicycle," *IEEE Trans. Control Syst. Technol.*, vol. 17, no. 3, pp. 658–670, May 2009.
[2] M.-H. Hsieh, Y.-T. Chen, C.-H. Chi, and J.-J. Chou, "Fuzzy sliding mode control of a riderless bicycle with a gyroscopic balancer," in *Proc. IEEE Int. Symp. Robotic Sensors Environ. (ROSE)*, Oct. 2014, pp. 13–18.
[3] C. Yang and T. Murakami, "Full-speed range self-balancing electric motorcycles without the handlebar," *IEEE Trans. Ind. Electron.*, vol. 63, no. 3, pp. 1911–1922, Mar. 2016.
[4] C.-H. Chi and J.-J. Chou, "Riderless bicycle with gyroscopic balancer controlled by FSMC and AFSMC," in *Proc. 7th Int. Congr. Ultra Modern Telecommun. Control Syst. Workshops (ICUMT)*, Oct. 2015, pp. 150–157.
[5] J. He, M. Zhao, and S. Stasinopoulos, "Constant-velocity steering control design for unmanned bicycles," in *Proc. IEEE Int. Conf. Robot. Biomimetics (ROBIO)*, Dec. 2015, pp. 428–433.
[6] C. Yang, Z. Li, R. Cui, and B. Xu, "Neural network-based motion control of an underactuated wheeled inverted pendulum model," *IEEE Trans. Neural Netw. Learn. Syst.*, vol. 25, no. 11, pp. 2004–2016, Nov. 2014.
[7] J. Huang, S. Ri, L. Liu, Y. Wang, J. Kim, and G. Pak, "Nonlinear disturbance observer-based dynamic surface control of mobile wheeled inverted pendulum," *IEEE Trans. Control Syst. Technol.*, vol. 23, no. 6, pp. 2400–2407, Nov. 2015.
[8] S. Liu and D. Sun, "Minimizing energy consumption of wheeled mobile robots via optimal motion planning," *IEEE/ASME Trans. Mechatronics*, vol. 19, no. 2, pp. 401–411, Apr. 2014.
[9] V. Muralidharan and A. D. Mahindrakar, "Position stabilization and waypoint tracking control of mobile inverted pendulum robot," *IEEE Trans. Control Syst. Technol.*, vol. 22, no. 6, pp. 2360–2367, Nov. 2014.
[10] H. K. Lam, C. Liu, L. Wu, and X. Zhao, "Polynomial fuzzy-model-based control systems: Stability analysis via approximated membership functions considering sector nonlinearity of control input," *IEEE Trans. Fuzzy Syst.*, vol. 23, no. 6, pp. 2202–2214, Dec. 2015.
[11] W. He, Y. Chen, and Z. Yin, "Adaptive neural network control of an uncertain robot with full-state constraints," *IEEE Trans. Cybern.*, vol. 46, no. 3, pp. 620–629, Mar. 2016.
[12] H. Zhou, H. Deng, and J. Duan, "Hybrid fuzzy decoupling control for a precision maglev motion system," *IEEE/ASME Trans. Mechatronics*, vol. 23, no. 1, pp. 389–401, Feb. 2018.
[13] J. Yu, P. Shi, W. Dong, and H. Yu, "Observer and command-filter-based adaptive fuzzy output feedback control of uncertain nonlinear systems," *IEEE Trans. Ind. Electron.*, vol. 62, no. 9, pp. 5962–5970, Sep. 2015.
[14] M. Tanaka, M. Nakajima, Y. Suzuki, and K. Tanaka, "Development and control of articulated mobile robot for climbing steep stairs," *IEEE/ASME Trans. Mechatronics*, vol. 23, no. 2, pp. 531–541, Apr. 2018.
[15] C.-F. Hsu and Y.-C. Chen, "Microcontroller-based B-Spline neural position control for voice coil motors," *IEEE Trans. Ind. Electron.*, vol. 62, no. 9, pp. 5644–5654, Sep. 2015.
[16] Y. Wang, R. Xiong, H. Yu, J. Zhang, and Y. Liu, "Perception of demonstration for automatic programing of robotic assembly: Framework, algorithm, and validation," *IEEE/ASME Trans. Mechatronics*, vol. 23, no. 3, pp. 1059–1070, Jun. 2018.
[17] L. de la Torre, M. Guinaldo, R. Heradio, and S. Dormido, "The ball and beam system: A case study of virtual and remote lab enhancement with moodle," *IEEE Trans. Ind. Informat.*, vol. 11, no. 4, pp. 934–945, Aug. 2015.

[18] R. Datta, S. Pradhan, and B. Bhattacharya, "Analysis and design optimization of a robotic gripper using multiobjective genetic algorithm," *IEEE Trans. Syst., Man, Cybern., Syst.*, vol. 46, no. 1, pp. 16–26, Jan. 2016.
[19] J. Huang, M. Ri, D. Wu, and S. Ri, "Interval Type-2 fuzzy logic modeling and control of a mobile two-wheeled inverted pendulum," *IEEE Trans. Fuzzy Syst.*, vol. 26, no. 4, pp. 2030–2038, Aug. 2018.
[20] H.-G. Han, X.-L. Wu, Z. Liu, and J.-F. Qiao, "Design of self-organizing intelligent controller using fuzzy neural network," *IEEE Trans. Fuzzy Syst.*, vol. 26, no. 5, pp. 3097–3111, Oct. 2018.
[21] C.-H. Chiu, Y.-F. Peng, and C.-H. Sun, "Intelligent decoupled controller for mobile inverted pendulum real-time implementation," *J. Intell. Fuzzy Syst.*, vol. 32, no. 6, pp. 3809–3820, May 2017.
[22] Y.-F. Peng, M.-H. Lin, and C.-M. Chong, "Design of output recurrent CMAC backstepping control system for tracking periodic trajectories," in *Proc. IEEE Int. Joint Conf. Neural Netw. Proc.*, Vancouver, BC, Canada, Jul. 2006, pp. 3108–3113.
[23] F.-J. Lin and Y.-C. Hung, "FPGA-based elman neural network control system for linear ultrasonic motor," *IEEE Trans. Ultrason., Ferroelectr., Freq. Control*, vol. 56, no. 1, pp. 101–113, Jan. 2009.
[24] J.-X. Xu, Z.-Q. Guo, and T. Heng Lee, "Design and implementation of a Takagi–Sugeno-type fuzzy logic controller on a two-wheeled mobile robot," *IEEE Trans. Ind. Electron.*, vol. 60, no. 12, pp. 5717–5728, Dec. 2013.

CHIH-HUI CHIU was born in Taiwan. He received the B.S. degree in electrical engineering from the Tatung Institute of Technology, Taipei, Taiwan, in 1994, and the M.S. and Ph.D. degrees in electrical engineering from National Central University, Taiwan, in 1996 and 2000, respectively. He is currently a Professor with the Department of Communications, Navigation and Control Engineering, National Taiwan Ocean University, Keelung, Taiwan. His research interests include fuzzy logic theory, intelligent control, robot, mechatronics, and control theory applications.

CHI-YUAN WU was born in Taiwan. He received the B.S. and M.S. degrees in electrical engineering from Yuan Ze University, Taoyuan, Taiwan. His research interests include fuzzy logic theory, intelligent control, and control theory applications.